ELSEVIER

Ab initio density functional study of O on the Ag(0 0 1) surface

M. Gajdoš, A. Eichler *, J. Hafner

Institut für Materialphysik and Center for Computational Materials Science, Universität Wien, Sensengasse 8/12, A-1090 Wien, Austria

Abstract

The adsorption of oxygen on the Ag(1 0 0) is investigated by means of density functional techniques. Starting from a characterization of the clean silver surfaces oxygen adsorption in several modifications (molecularly, on-surface, sub-surface, Ag_2O) for varying coverage was studied. Besides structural parameters and adsorption energies also work-function changes, vibrational frequencies and core level energies were calculated for a better characterization of the adsorption structures and an easier comparison to the rich experimental data.
© 2003 Elsevier Science B.V. All rights reserved.

Keywords: Density functional calculations; Silver; Oxygen; Chemisorption; Oxidation

1. Introduction

Despite the progress realized in surface science during the last decades, there are still unsolved questions for processes as elementary as atomic adsorption. One particular example is the adsorption of oxygen on the Ag(0 0 1) surface.

Already an early work-function study [1] indicates a non-trivial adsorption behavior: while the work-function increases monotonically with oxygen coverage for the (1 1 0) surface of silver, the work-function change for the (0 0 1) surface depends not only on coverage, but also on temperature. For surface temperatures higher than about 320 K oxygen exposure results always in an increased work-function, whereas at lower tem-

peratures only small oxygen doses lead to a positive work-function change. For higher exposure the work-function decreases upon oxygen adsorption. Later this "phase transition" between a high- and a low-temperature structure could be reproduced and the different phases characterized by high resolution electron energy loss spectroscopy (HREELS) and low-energy electron diffraction (LEED) [2]. Very recently these results were confirmed by a combined LEED, HREELS, X-ray photoemission spectroscopy (XPS) and X-ray photo-electron diffraction (XPD) study [3]. Upon oxygen exposure several distinct species can be prepared (comp. Table 1):

(1) Adsorption at low temperature ($T < 150$ K) leads to a molecular species, which is stable up to 200 K and has been well characterized by XPD [3], HREELS [7] and thermal desorption spectroscopy (TDS) [8]. According to a scanning tunnelling microscopy (STM) study, the molecules adsorb in hollow sites, forming a $c(2 \times 4)$ structure [6].

---

* Corresponding author. Tel.: +43-1-427751402; fax: +43-1-42779514.

E-mail addresses: marek.gajdos@univie.ac.at (M. Gajdoš), andreas.eichler@univie.ac.at (A. Eichler).

Table 1
Experimental characterization of the different oxygen adsorption phases on Ag(0 0 1): O 1s binding energies E_b(O 1s), Ag–O stretching frequencies hv, LEED pattern, work-function change $\Delta\Phi$ and estimated height of O above the surface h_O

	$T < \sim 200$ K	$T < \sim 320$ K	$T > \sim 320$ K
E_b(O 1s) (eV)	532.2	530.3(530.9)	528.3
hv (meV)	30,84	34–37 (131)	28–31
LEED/STM	c(2 × 4)	c(2 × 2)	p(1 × 1)
$\Delta\Phi$ (eV)	–	~-0.2	~ 0.3
h_O (Å)	–	−0.15	0.6

The results for atomic oxygen are taken from Refs. [1–5], those for molecular oxygen ($T < 200$ K) from Refs. [6,7].

(2) After dissociation atomic oxygen adsorbs at the surface with an O 1s binding energy of 530.3 eV and a vibrational frequency of about 30 meV. At around 190 K a sharp c(2 × 2) pattern appears and the frequency shifts up to 36 meV. An additional loss at 131 meV has been assigned recently on the basis of isotopically labelled oxygen to an electronic transition [5]. Based on XPD a missing-row p($2\sqrt{2} \times \sqrt{2}$) reconstruction of the substrate was proposed (with the oxygen atoms forming a c(2 × 2) arrangement) [3].

(3) Heating of this structure above $\sim$320 K lifts the reconstruction, the O 1s binding energy changes from 530.3 to 528.3 eV and the vibrational frequency decreases again from 34–37 to 28–31 meV [3].

(4) Around the transition temperatures also an additional oxygen moiety appears with a binding energy of 530.9 eV [3], which vanishes already at 350 K and could have been shadowed for lower temperatures by the dominant peak at 530.3 K. This species has been assigned to sub-surface oxygen.

Interestingly only the higher temperature species characterized by an O 1s binding energy at 528.3 eV is active towards CO and C_2H_4 oxidation [3]. Based on the structural models from XPD, a combined ab initio and ultraviolet photoemission spectroscopy study was devoted to the investigation of electronic surface states [9]. In a recent STM experiment three different species of adsorbed oxygen ($T_{ads} = 150$ K) are reported for low coverage ($\Theta_O \sim 0.1$ ML) and assigned to hollow, bridge and on-top adsorbed atoms [10]. Finally, last year two density functional studies appeared investigating the oxygen adsorption on the Ag(0 0 1) [11,12]. Both studies are in a good agreement with our study. Also the adsorption on Ag(1 1 1) surface was

investigated recently via density functional theory (DFT) techniques [13,14].

In the present study we use DFT calculations to gain further insight into this complicated adsorption behavior. First we present our results for the clean silver surface. Then we discuss adsorption of oxygen in high symmetry (on-surface) sites of the (0 0 1) surface at different O-coverage. Subsequently results for molecular adsorption, the proposed missing-row reconstruction and the silver oxide surface are presented. The paper closes with a discussion of our results in the light of the experimental data.

2. Methodology

The calculations are performed using the Vienna ab initio simulation package (VASP) [15, 16] which is a DFT code, operating in a plane-wave basis set. The electron–ion interaction is described using the projector-augmented-wave method [17,18] with plane waves up to an energy of $E_{cut} = 250$ eV. For exchange and correlation the functional proposed by Perdew and Zunger [19] is used, adding (non-local) generalized gradient corrections (GGA) following Perdew et al. [20]. If not mentioned differently we have used a (12 × 12 × 1) k-points mesh for the integration over the Brillouin zone for the p(1 × 1) cell, (6 × 6 × 1) for c(2 × 2), (4 × 4 × 1) for p(2 × 2) and a (3 × 3 × 1) mesh for a p(3 × 3) cell.

The system itself is modelled by six layers of Ag separated by 14 Å of vacuum with oxygen adsorbed on one side of the slab. The upper two layers of the Ag surface are allowed to relax, the remaining atoms are fixed at their ideal bulk positions ($a_{GGA} = 4.16$ Å, $a_{exp} = 4.08$ Å).

The free molecule is characterized by a calculated stretch frequency of 1561 cm^{-1} at an equilibrium bond length of 1.23 Å. The corresponding experimental values are 1580 cm^{-1} and 1.21 Å [21]. The problematic description of the O_2 binding energy ($E_{O_2}^{GGA} = 6.25$ eV, $E_{O_2}^{exp} = 5.23$ eV) stems mainly from the error in the energy of the free atoms, where high density gradients make an accurate description more difficult. So the reported energies (with respect to the calculated binding energy of molecular oxygen) should be of much higher accuracy. This is for example reflected by the calculated formation energy for Ag_2O of 0.39 eV compared to the literature value of 0.32 eV [22].

Adsorbate–substrate stretching frequencies have been obtained from finite displacements of the oxygen atoms along all three Cartesian directions ($\Delta = \pm 0.04$ Å). In order to increase the accuracy we performed the calculations with a harder pseudo-potential requiring an energy cut-off of $E_{cut} = 400$ eV. Diffusion barriers were determined with the nudged elastic band (NEB) method [23,24].

Core-level shifts were calculated in a $(2\sqrt{2} \times \sqrt{2})$ cell sampled by a $(3 \times 6 \times 1)$ k-points mesh. Further details concerning the calculation of the core levels (final state effects) are given in Ref. [25].

3. Results

3.1. Clean Ag(0 0 1)

The clean Ag(0 0 1) surface is well characterized, experimentally as well as theoretically [11,12,26–31]. Calculations have been done for slabs with 4–8 layers, to check for errors due to the finite thickness of the Ag film. Both surfaces of the slab were relaxed. Table 2 compiles our results for inter-layer relaxation, surface energy and work-function together with values from the literature. We find that structural, as well as electronic parameters agree well with earlier results. A slight inward relaxation of the surface plane is compensated by outward relaxations of the lower layers of comparable size. The surface energy is underestimated by about 30% compared to earlier LDA calculations and experiments, a property of the GGA that has already been discussed earlier [32]. However, since it is well established that the GGA leads to a more reliable description of the adsorption process we did our calculations with the inclusion of gradient corrections.

Concerning the slab thickness dependence, results for the six layer slab, which were used for the adsorption studies are converged within 0.1% (0.02 Å) for the inter-layer relaxation, within 30 mJ/m^2 for surface energies and the work-function varies only by 60 meV when going from six to eight layers.

3.2. Adsorption in high symmetry on-surface sites

As a first step towards a deeper understanding of the adsorption process, we put oxygen at varying coverage ($\Theta = 1/9, 1/4, 1/2, 3/4, 1$ ML) in the high symmetry positions (top, bridge, hollow) of the slab, optimized the geometry and calculated frequencies and work-function changes. For the characterization of the energy balance during adsorption we chose two slightly distinct

Table 2

Inter-layer relaxation (Δd_{12}, Δd_{23}, Δd_{34}) in %, surface energy (σ) in J/m^2 and work-function (Φ) in eV for a clean Ag(0 0 1) surface as a function of slab thickness

	Present work (GGA)			Theory (LDA)	(GGA)[a]	(GGA)[b]	Exp.
	Number of layers						
	4	6	8				
Δd_{12} [%]	−1.9	−1.6	−1.5	−1.3[c]	−2.0	−1.7	0 ± 1.5[d]
Δd_{23} [%]	0.3	0.7	0.8	1.0[c]	0.8	0.7	0 ± 1.5[d]
Δd_{34} [%]	–	0.8	0.9	0.8[c]	–	0.2	–
σ [J/m^2]	0.82	0.80	0.78	1.21[c]	0.8	–	1.27[e]
Φ [eV]	4.22	4.38	4.44	4.43[f]	4.62	4.33	4.42[g]

Earlier theoretical and experimental results are taken from Refs. [11] (a); [12] (b); [27] (c); [29] (d); [30] (e); [28] (f); [31] (g).

quantities. First, the adsorption energy per adsorbed atom (E_{ads}) with respect to half an oxygen molecule defined as

$$E_{ads} = \left(E_{tot} - E_{clean} - \frac{N_O}{2} \cdot E_{O_2} \right) \Big/ N_O, \qquad (1)$$

with the total energy of the adsorption system (containing N_O oxygen atoms) E_{tot}, the energy of the clean surface (E_{clean}) and the energy of a free O_2 molecule E_{O_2}. Following this definition, E_{ads} decreases (i.e. becomes more exothermic) with increasing Ag–O bond strength. Secondly, we use a (generalized) surface energy per area A (especially for the comparison with the reconstructed missing-row structure, discussed below)

$$\sigma = \left(E_{tot} - N_{Ag} \cdot E_{Ag} - \frac{N_O}{2} \cdot E_{O_2} \right) \Big/ A - \sigma_{clean}, \qquad (2)$$

where N_{Ag} and E_{Ag} are the number of silver atoms per cell and the total energy of a bulk silver atom, respectively. The subtraction of the surface energy of a clean silver surface σ_{clean} accounts for the second (uncovered) surface of the slab. This surface energy describes the energy cost for creating a surface minus the energy gain due to oxygen adsorption.

The results for the various adsorption sites at different coverage are compiled in Table 3; Fig. 1 gives a graphical summary of the adsorption energy versus adsorption height. At every coverage, adsorption in hollow sites is favored while on-top and bridge adsorption is nearly always endothermic. Only at a coverage of $\Theta = 0.25$ ML adsorption in bridge sites becomes thermoneutral, but remains still ≈ 0.8 eV less favorable compared to adsorption in the hollow sites. All these findings for the adsorption energetics are in nice agreement with two recent DFT studies [11,12]. This strong preference of hollow adsorption makes the interpretation of the STM images in Ref. [10] in terms of bridge- and top-adsorbed meta-stable oxygen species very improbable, unless there were huge barriers between the adsorption sites. This point will be addressed in the following section.

At full coverage we performed additionally spin-polarized calculations. For atop adsorption a substantial magnetic moment of the O atom of

Table 3
Results for oxygen adsorbed in high symmetry sites (t—top, b—bridge, h—hollow) on Ag(001) for coverages varying between $\Theta = 0.11$ and 1 ML

	p(1×1)O; $\Theta=1$ ML			p(2×2)3O; $\Theta=0.75$ ML			c(2×2)O; $\Theta=0.5$ ML			p(2×2)2O; $\Theta=0.25$ ML			p(3×3)O; $\Theta=0.11$ ML		
	t	b	h	t	b	h	t	b	h	t	b	h	t	b	h
σ [J/m²]	3.54	2.33	0.52	2.72	1.73	0.48	1.83	1.04	0.15	1.24	0.75	0.38	1.00	0.77	0.62
E_{ads} [eV]	1.48	0.83	-0.14	1.42	0.70	-0.20	1.11	0.26	-0.71	1.06	-0.00	-0.80	1.14	0.03	-0.72
h [Å]	2.04	1.39	-0.33	1.91	1.55	0.14	1.56	1.32	0.69	1.88	1.40	0.81	1.88	1.38	0.71
Δd_{12} [%]	-1.1	-0.4	31.1	-0.8	-1.5	14.5	6.4	-1.9	4.8	-1.4	-1.2	-0.8	-1.6	-1.7	-1.6
b_1 [Å]	0	0	0	0.22	0.08	0	0.77	0	0	0.13	0.07	0	0.04	0.06	0.03
Δd_{23} [%]	0.2	-0.3	-0.4	-0.4	2.8	-1.6	-1.9	-1.3	-0.8	-0.1	0.5	-1.0	0.6	0.1	1.4
b_2 [Å]	0	0	0	0	0.08	0.1	0	0	0.03	0	0.01	0.14	0.02	0.03	0.11
d_{Ag-O} [Å]	2.04	2.02	2.11	2.00	2.09	2.10	1.95	2.05	2.19	1.96	2.07	2.26	1.97	2.07	2.26
$\Delta\Phi$ [eV]	4.44	4.04	-0.14	3.91	3.29	0.47	3.30	3.22	0.94	1.96	1.69	0.68	1.18	0.87	0.34
ν [meV]	53.5	52.8	23.3	51.5	45.2	26.1	67.6	51.3	29.4	64.6	50.0	30.8	63.0	48.0	24.2

The reported quantities are: σ—surface energy; E_{ads}—adsorption energy; h—height of O with respect to the average surface plane atoms; Δd_{12}, Δd_{23}—change of the average inter-layer spacing; b_1, b_2—buckling of first and second layer; d_{Ag-O}—minimal Ag–O distance; $\Delta\Phi$—oxygen induced work-function change; ν—oxygen frequency perpendicular to the surface.
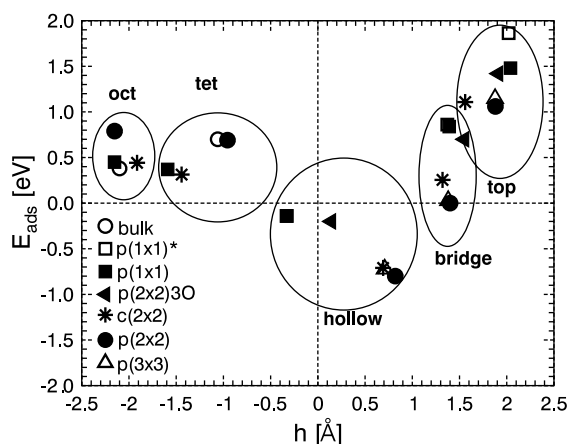
Fig. 1. Adsorption energy (E_{ads}) versus height of the adsorbed O atom for various adsorption sites and coverage. The second data set for full coverage (denoted by an asterisk) has been obtained from a spin polarized calculation. For subsurface adsorption also energies for incorporation in bulk Ag are included (empty circles).

1.4 μ_B persists, leading to a decrease in the adsorption energy by -0.4 eV at an unchanged geometry. In the higher coordinated sites the effect of spin polarization is negligible, due to the stronger interaction with the substrate. At lower coverage this effect is expected therefore to be even smaller due to stronger Ag–O interaction, justifying the neglect of spin polarization in further calculations.

The inward relaxation of the first substrate layer, which was observed for the clean surface, persists up to a coverage of $\Theta = 1/4$ ML; for higher coverage it is gradually turned into an expansion. For the second inter-layer spacing the sign of the relaxation changes already at $\Theta = 1/4$ ML. The adsorption heights for the three high symmetry adsorption sites vary such, that the Ag–O bond length remains always between 1.9 and 2.3 Å. This results in adsorption heights of around 2.0, 1.4 and 0.7 Å for top, bridge and hollow adsorption, respectively. The correlation between adsorption energy and adsorption height reveals a very peculiar character of O-adsorption in the hollow position (see Fig. 1). Whereas for bridge- and top-adsorbed O the adsorption-height is almost independent of the coverage and the adsorption energy becomes more endothermic as the coverage increases, hollow-adsorbed O sinks dee-

per into the surface with increasing coverage—at full coverage the stable adsorption sites are located even below the surface-plane ($h_{\Theta=1} = -0.33$ Å). This reduction of the adsorption-height is accompanied by a strong outward relaxation of the top Ag-layer ($\Delta d_{12} = 31\%$). This expanded adsorption structure may be interpreted as the formation of an silveroxide layer which is weakly bonded to the Ag-substrate. A similar behavior is found already for $\Theta = 3/4$ ML ($p(2 \times 2)3O$). In this structure two inequivalent adsorption sites exist for oxygen. Two out of three oxygen atoms are equivalent due to symmetry and stay above the surface at a height of $h = 0.26$ Å, while the third oxygen atom sinks below the first layer ($h = -0.09$ Å).

The work-function change $\Delta\Phi$ for top and bridge adsorbed oxygen increases monotonically with coverage. For the hollow site this trend holds only up to 1/2 ML, from where on $\Delta\Phi$ decreases again, due to the aforementioned negative adsorption heights at 0.75 and 1 ML.

The vibrational frequency perpendicular to the surface exhibits for all three adsorption sites an increasing trend with coverage up to around 0.5 ML. From there on the vibrational modes become softer again due to the pronounced weakening of the Ag–O bond at high coverage.

3.3. Transition between high-symmetry sites—surface diffusion

In a recent low temperature STM study [10] three different oxygen species have been imaged for low oxygen coverage. These have been assigned to hollow adsorbed oxygen atoms and two metastable species residing in bridge and on-top sites, respectively. Considering the large differences in the adsorption energies for these three sites, this could only be possible if there were significant barriers separating the meta-stable sites from the hollow position. In order to clarify this point we performed NEB [23,24] calculations to determine the diffusion barriers between neighboring high symmetry sites. Fig. 2 shows the variation of the potential energy for the movement of an oxygen atom from a bridge-site via hollow towards the on-top position, following the pathway shown in the inset. For this calculation (performed in a $p(2 \times 2)$
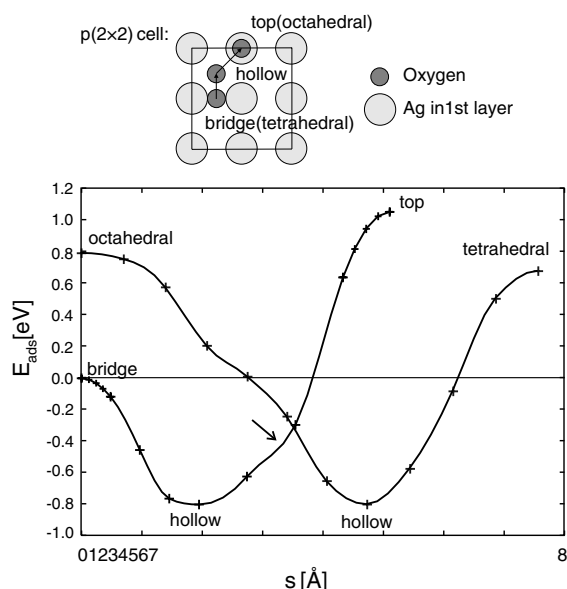
Fig. 2. Adsorption energy E_{ads} along a pathway connecting the adsorption sites bridge–hollow–top calculated in a 2×2 cell (octahedral–hollow–tetrahedral sites for the pathway leading into subsurface positions; compare sketch). Calculated points are indicated by crosses, the connecting lines are spline fits, based on forces.

cell) again the upper two silver layers were allowed to relax.

The results show that bridge and on-top sites are only saddle-points of the potential energy surface for this coverage. Hence on the basis of these findings the interpretation given in the STM work becomes very improbable. However, the calculation reveals another possible (threefold) adsorption site between hollow and on-top, reflected by a dip along the pathway (arrow in the graph on Fig. 2). For a further investigation we put the oxygen atom artificially at that position and performed again a structural optimization. Our calculations did not lead to any local minimum.

3.4. Sub-surface adsorption

We have also considered the sub-surface adsorption of oxygen, since such species are believed to be important for the selectivity of silver in catalyzing ethylene epoxidation [33]. We investigated the sub-surface adsorption for coverages between a quarter and full monolayer (p(2×2), c(2×2) and p(1×1) structures) in the octahedral and tetrahedral sites, the results of which are compiled in Table 4 and Fig. 1. For comparison, we included in Fig. 1 also the energies for oxygen incorporated in the tetrahedral and octahedral sites of bulk Ag (in a $3 \times 3 \times 3$ cell). Sub-surface adsorption is an endothermic process compared to molecular O_2 at all investigated coverages (see Fig. 1). However, there are interesting trends of the adsorption

Table 4
Results for oxygen adsorbed in the octahedral (oct) and tetrahedral (tet) sub-surface sites at coverages of 1 ML (p(1×1)), 0.5 ML (c(2×2)) and 0.25 ML (p(2×2))

	p(1×1); $\Theta = 1$ ML		c(2×2); $\Theta = 0.5$ ML		p(2×2); $\Theta = 0.25$ ML	
	oct	tet	oct	tet	oct	tet
σ [J/m^2]	1.65	1.49	1.24	1.12	1.13	1.08
E_{ads} [eV]	0.46	0.37	0.44	0.31	0.79	0.69
Δd_{12} [%]	50.4	54.2	35.6	44.9	8.7	16.0
b_1 [Å]	0	0	0.58	0	0.42	0.64
Δd_{23} [%]	0.9	−0.9	1.4	0.6	3.0	−0.5
b_2 [Å]	0	0	0	0	0	0.12
d_{Ag-O}^u [Å]	2.15	2.17	2.21	2.15	2.38	2.10
d_{Ag-O}^m [Å]	2.30	–	2.27	–	2.23	–
d_{Ag-O}^l [Å]	3.07	2.19	3.02	2.20	2.32	2.18
$\Delta \Phi$ [eV]	0.15	0.37	0.15	0.37	0.27	0.15
v [meV]	34.2	37.4	36.0	48.8	29.5	49.6

The reported quantities are: σ—surface energy; E_{ads}—adsorption energy; Δd_{12}, Δd_{23}—change of the average inter-layer spacing; b_1, b_2—buckling of first and second layer; d_{Ag-O}^u, d_{Ag-O}^m, d_{Ag-O}^l—shortest Ag–O distance to the upper, middle and lower Ag layer; $\Delta \Phi$—the work function change compared to the clean Ag(0 0 1) surface and the oxygen frequency perpendicular to the surface v.

energy in coverage and in comparison to the dilute solution of oxygen in the bulk. In contrast to the on-surface adsorption the variation of the adsorption energy with coverage is non-monotonous, the smallest (least endothermic) energy is calculated for $\Theta = 0.5$ ML, i.e. at a composition of the surface layer corresponding to stoichiometric Ag_2O. And the dilute solution of oxygen in bulk silver is an extremum for both adsorption sites: for the octahedral site it is more stable than the high coverage subsurface case, whereas the tetrahedral interstitial is even less stable than the quarter coverage subsurface position.

This peculiar behavior can be understood when considering the geometries of the two interstitial sites. Placing an oxygen atom into an ideal (unrelaxed) Ag bulk leads to Ag–O bond lengths of 1.80 Å for the tetrahedral and 2.08 Å for the octahedral site. So compared to the typical Ag–O bond lengths of 2.0–2.2 Å (compare Table 3) the octahedral site can easily accommodate an oxygen atom, whereas the tetrahedral site is too small. This explains already the strong preference for the octahedral site in the dilute solution of oxygen in the bulk. At the surface the incorporation of oxygen induces pronounced geometrical changes, partially just for sterical reasons, so that the site becomes large enough to accommodate the additional atom; partially because the formation of strong Ag–O bonds weakens the Ag–Ag bonds and leads hence to an outwards relaxation of the first layer.

For the larger octahedral site, the second contribution dominates: already at the lowest coverage (p(2×2)), the outward relaxation together with the up-shift of the immediate silver neighbor in the first layer (reflected by a large buckling of 0.42 Å), expands the octahedral site such that two of the six Ag–O bonds increase beyond 2.3 Å and are significantly weakened. This results in the weakest subsurface adsorption energy of this study. With increasing coverage, the outward relaxation increases dramatically, so that a slightly different adsorption geometry between the first and second layer becomes available. In this position the Ag—bond to the third layer is now completely absent ($d_{Ag-O}^{l} > 3$ Å), but for that the remaining five bonds are stronger and make this position lower in energy.

The smaller tetrahedral site on the other hand has to rely on the (local) expansion of the substrate. At low coverage the two silver neighbors in the first layer have to shift up significantly (leading to a buckling of 0.64 Å), so that the interstitial becomes large enough. Such a large distortion costs energy and makes the tetrahedral site unfavorable at low coverage. With increasing coverage, the weakening of the Ag–Ag bonds opens up the first interlayer spacing, so that adsorption in the tetrahedral site becomes not only possible, but even more favorable than adsorption in the octahedral site.

The vibrational frequencies perpendicular to the surface for the tetrahedral and octahedral site are remarkably similar to those for the corresponding on-surface sites, bridge and hollow, respectively.

Similar to the on-surface case we calculated the potential energy along a pathway connecting the subsurface sites with the on-surface hollow position in a p(2×2) cell. The monotonic decrease in energy towards the hollow position demonstrates that isolated sub-surface sites are highly unstable at this coverage and can only be stabilized by co-adsorbed on-surface oxygen, preventing the migration back to the surface.

3.5. Missing-row reconstruction

For the low-temperature phase (below 320 K, compare Table 1), a missing-row reconstructed phase with a p(2√2 × √2) periodicity has been proposed by Rocca et al. on the basis of XPD experiments [3]. The still rather regular position of the oxygen atoms should give rise to the observed c(2×2) LEED pattern [2].

Starting from the proposed geometry we optimized the structure for the missing-row reconstruction (see Fig. 3). However, in the structure proposed on the basis of the XPD experiments the oxygen atoms are 0.15 Å below the average of the surface plane and laterally shifted by 0.36 Å towards the missing rows [3], at variance to our results.

In the relaxed configuration the oxygen atoms are located at a height of about 0.13 Å above the average surface plane in the pseudo-hollow
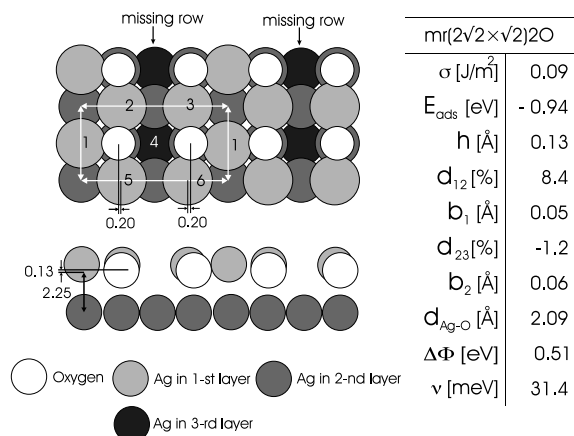
Fig. 3. Results for the $(2\sqrt{2} \times \sqrt{2})$ missing-row reconstruction with two oxygen atoms in the pseudo-threefold hollows. The sketch shows a top and side view of the optimized structure (all distances in Å). The reported quantities in the table are: σ—surface energy; E_{ads}—adsorption energy with respect to a clean reconstructed surface; h—height of O with respect to the average surface plane; Δd_{12}, Δd_{23}—change of the average inter-layer spacing; b_1, b_2—buckling of first and second layer; d_{Ag-O}—minimal Ag–O distance; $\Delta\Phi$—oxygen induced work-function change; ν—vibrational frequency perpendicular to the surface.

sites along the missing-rows; the under-coordinated Ag atoms move by ~0.2 Å towards the missing-rows, leading to a structure comparable to what is observed for O on Cu(0 0 1) [34,35]. Very similar results were obtained in the recent theoretical studies by Cipriani et al. [11] and Wang et al. [12].

Besides the differences in structure, the reconstructed phase also cannot account for other properties observed for the low temperature phase. Experimentally this phase should be characterized by an increased vibrational frequency around 34–37 meV [3,5] and a negative work function change [1], compared to the calculated values of 31 meV for the frequency and a work function change of $\Delta\Phi = +0.5$ eV.

From an energetic point of view (surface energy), this reconstructed structure is very similar to the simple c(2×2) structure. In order to minimize any errors due to differences in the setup (k-points, grids for Fourier transformations) we recalculated both structures (the c(2×2) and the missing row structure) in a $(2\sqrt{2} \times \sqrt{2})$ cell with a denser k-point mesh ($5 \times 10 \times 1$). Using this setup,

the surface energy (calculated according to Eq. (2)) for the reconstructed structure is even slightly lower in energy ($\Delta\sigma = 50$ mJ/m²), so that within the accuracy of our calculation both structures are essentially degenerate.

Hence, although oxygen adsorption leads indeed to a strong weakening of the Ag–Ag bonds, so that structures such as the missing-row reconstruction become energetically possible, this particular structure is not consistent with the experimental findings. A way out of this dilemma would be a more complicated structure with additional sub-surface oxygen, as it was already argued in Refs. [3,5]. Therefore we tested several combinations of occupied octahedral and tetrahedral sub-surface sites together with the experimentally proposed pseudo-hollow site along the missing-rows (see Table 5). However, neither of these structures can either account satisfactorily for the observed experimental structure nor is energetically more favored than the simple missing row reconstruction.

3.6. Molecular adsorption

Adsorption below 150 K leads to molecular adsorption of oxygen [7,36]. At low coverage two

Table 5
Several combinations of sub-surface oxygen(s) in the missing-row $(2\sqrt{2} \times \sqrt{2})$ cell in addition to two oxygens in the pseudo-hollows (comp. Fig. 3)

Sub-surface oxygens	Θ [ML]	E_{ads} [eV]	σ [J/m²]
–	0.50	−0.94	0.09
oct (1)	0.75	−0.69	0.10
tet (2–4)	0.75	−0.32	0.61
oct (1), (2)	1.00	−0.50	0.13
tet (1–5), (3–1)	1.00	−0.37	0.36
oct (1), (2), (3)	1.25	−0.34	0.28
tet (6–1), (1–2), (5–4)	1.25	0.17	1.28
oct (1), (2), (3), (4)	1.50	−0.14	0.59
tet (3–4), (4–6), (1–3), (1–6)	1.50	0.16	1.41

The first column describes the position of the sub-surface atoms by the atom number (according to Fig. 3) of the nearest on-surface atoms. Tetrahedral sites (tet) are between first and second layer, octahedral sites (oct) in the second layer. Compiled is the resulting total coverage Θ, the adsorption energy with respect to a clean reconstructed surface E_{ads} and the generalized surface energy σ.

distinct molecular species could be identified via vibrational spectroscopy [36]. However, since already for coverages as low as 0.15 ML one species starts to dominate significantly, we will concentrate in the following only on this moiety, which saturates finally in a c(2 × 4) structure, as observed by STM [6]. By comparison with tight binding molecular dynamics simulations with these STM results the fourfold hollow site was proposed as adsorption site with the molecular axis oriented towards the neighboring bridge sites. The analysis of thermal desorption spectra [8] lead to an estimate for the adsorption energy of 0.4 eV. This molecular species is further characterized via two dipole active modes at 84 meV and 30 meV [7] and an O 1s core binding energy of around 532.2 eV [3] (comp. Table 1). We tested several molecular adsorption configurations. The most stable position of the molecule is over a hollow site, with the molecular axes oriented towards the bridge positions, in agreement with the proposed structure from Ref. [6] (Fig. 4). In the c(2 × 4) structure (i.e. 0.25 molecules per substrate atom) every silver atom binds to only one molecule, so that a quite strong binding is possible. The results of our calculation are
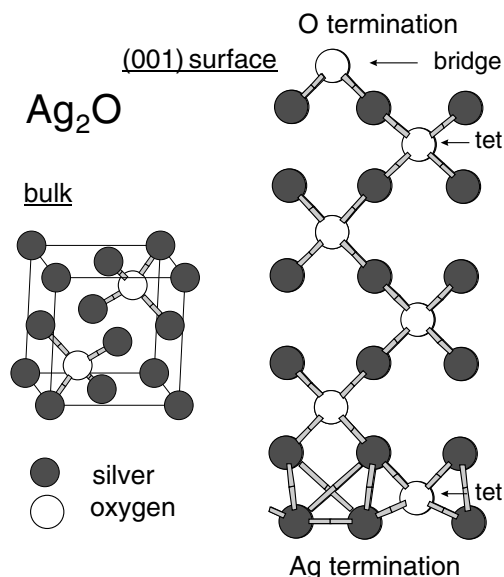
Table 6

Results for molecular oxygen adsorbed in the hollow sites of Ag(0 0 1) (with the molecular axis pointing towards the bridge sites) in a c(2 × 4) structure

	O_2: c(2 × 4)
σ [J/m^2]	0.50
E_{ads} [eV]	−0.68
d [Å]	1.43
h [Å]	1.47
Δd_{12} [%]	−0.7
b_1 [Å]	0
Δd_{23} [%]	+1.1
b_2 [Å]	0.06
$\Delta \Phi$ [eV]	1.83
v_{O-O} [meV]	97
v_{M-O_2} [meV]	29
$v_{frust. rot.}$ [meV]	39, 38
$v_{frust. trans.}$ [meV]	28, 19

The reported quantities are: σ—surface energy; E_{ads}—adsorption energy per molecule, molecular bond length (d) and height above the surface plane (h); Δd_{12}, Δd_{23}—change of the average inter-layer spacing; b_1, b_2—buckling of first and second layer and the change of the work-function $\Delta \Phi$. The frequencies (v) correspond to intramolecular stretch, molecule-surface vibration, frustrated rotation perpendicular and parallel to the surface, and the two frustrated translations parallel to the surface.

compiled in Table 6. The molecule is stretched to a bond-length of 1.43 Å, situated 1.47 Å above the surface plane. Similar to atomic adsorption, the first interlayer spacing is reduced by −0.7%, whereas the second is slightly expanded (+1.1%). The magnetic moment of the molecule vanishes completely and the work-function of the surface is increased by 1.83 eV. The calculated adsorption energy (−0.68 eV per molecule) is significantly higher than the experimental estimate of −0.4 eV [8], reflecting the well known overestimation of adsorption energies even with the used gradient corrected exchange correlation functionals [37]. Also the frequencies are overestimated by about 15%. A possible reason for this could be the neglect of substrate movement when calculating the frequencies, which could be for a "soft" substrate with a low melting temperature like silver quite crucial.

3.7. Silver-oxide—Ag₂O

Since it is nowadays well established that on some metals the reactive surface is the oxidized

Fig. 4. Structure of silver oxide (Ag₂O) in the bulk and of the (asymmetrically terminated) (0 0 1) oriented surface slab, as it was used in the calculations.

one [38,39], we performed also a limited set of calculations for the (0 0 1) surface of Ag_2O, which is the stable oxide at room-temperature (see Fig. 4). The lattice constant as determined by the calculation is $a_{GGA} = 4.83$ Å ($a_{exp} = 4.72$ Å [40]). In the DFT silveroxide exhibits a vanishing energy gap and becomes hence metal-like [41] in contradiction to experimental findings, according to which Ag_2O should be a semiconductor. However, we hope that these shortcomings in the electronic description do not have a major influence on the results presented in the following.

For the modelling of the surface we chose a rather small super-cell with two silver atoms per layer and a total of six Ag-layers as sketched (after relaxation) in Fig. 4. With this setup we could model at the same time a silver terminated surface on one end of the slab and an oxygen terminated one on the other side. We fixed the innermost two layers at their ideal bulk position and optimized all other layers. The results are compiled in Table 7. Further results for this oxidic surface are given in the subsequent section.

3.8. Core level binding energies

The phase transition between the low-temperature and high temperature phase has been characterized mainly by core-level spectroscopy (XPS) [3] (comp. Table 1). In addition to the O 1s binding energies also the Ag 3d$_{5/2}$ core levels have been measured as function of coverage and temperature. Hence, we calculated also for some structures the binding energies of the core-levels. In these calculations vanishing screening was assumed, so that all electrons can simultaneously relax into the ground state, after the core electron was removed (final state effects) [25]. In order to minimize errors

Table 7
Results for the (0 0 1) surface of silver oxide (Ag_2O): Change of the inter-layer spacing (Δd) with respect to the ideal (bulk) Ag–O layer distance and the work-function Φ

	O-terminated	Ag-terminated
Δd_{12} [%]	−5.2	−44.1
Δd_{23} [%]	−14.4	+3.4
Δd_{34} [%]	−5.0	+5.8
Φ [eV]	6.98	4.38

due to different unit-cells, all calculations were performed within a the p($\sqrt{2} \times 2\sqrt{2}$) cell sampled by a grid of 6×3 k-points. Since the absolute values from the calculations are not well defined, only energy differences can be compared. For silver the bulk core level (calculated with in the same super cell) is an appropriate reference, for oxygen we chose hollow adsorption at low coverage ($\Theta = 0.25$ ML).

3.8.1. Ag 3d

Experimentally, for the Ag 3d$_{5/2}$ core level only two peaks could be resolved independent of temperature and oxygen coverage: one peak at 368.0 eV for the clean surface component and a second at 367.6 eV for silver atoms in contact with oxygen [3]. While for the low temperature phase both peaks are almost of equal intensity, the surface component clearly dominates at high temperatures. Fig. 5 summarizes the results of our calculations. On the clean surface the Ag 3d$_{5/2}$ energy is shifted by approximately 240 meV with respect to the bulk Ag core-level. With increasing oxygen coverage the binding energy shifts down, almost linearly with the number of oxygen neighbors, as it was observed already for oxygen on Ru(0 0 0 1) and Rh(1 1 1) [42]. Since already a single oxygen neighbor induces a shift (with respect to the clean surface) of about 0.25 eV, the experimentally
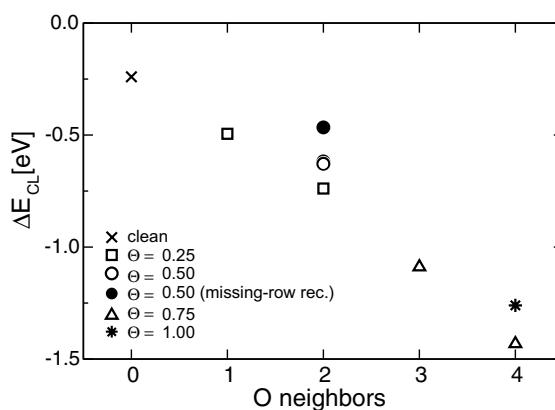
Fig. 5. Ag 3d surface core-level shifts as a function of the number of oxygen neighbors for different coverage. All values have been calculated in a p($2\sqrt{2} \times \sqrt{2}$) cell. The binding energy of bulk silver calculated in a comparable cell was taken as reference.

observed shift of −0.4 eV implies that there are no silver atoms with more than two oxygen neighbors. This is also in line with the experimental interpretation of a maximum coverage of 0.4 ML [3]. Slightly different is the situation for the missing row reconstruction. Here the reduced number of silver nearest neighbors shifts the core-level up by approximately 150 meV, thus compensating partially for the oxygen induced shift (comp. Fig. 5, full symbols).

3.8.2. O 1s

The experimental results for the oxygen 1s core-levels from Rocca et al. [3] are more complicated (comp. Table 1, Fig. 6): At lowest temperature the molecular species can be identified via its binding energy around 532.0 eV. Dissociation of the molecules leads to a prominent peak at 530.3 eV up to a temperature of around 300 K, where this peak starts to vanish. Prior to disappearing another small peak appears at approximately 530.9 eV, which could have been there already before, but buried by the main peak at 530.3 eV. This peak vanishes also at 350 K. Above 300 K the high-temperature species gives rise to a peak at around 528.3 eV.
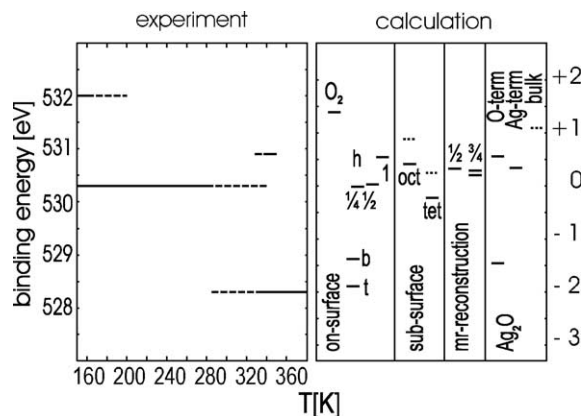

Fig. 6. Experimentally determined O 1s binding energies for varying temperature, taken from Ref. [3] (left panel). Calculated core-level binding energies for different coverages and adsorption geometries (right panel); numbers indicate the coverage in mono-layer, dashed lines refer to oxygen in bulk positions.

Table 8 summarizes the results for various structures and adsorption sites. All energies are given with respect to the O 1s binding energy of hollow-adsorbed oxygen at low coverage ($\Theta = 0.25$ ML). The core-level is mainly determined by the coordination of the adsorption site and changes hardly with coverage, as can be seen from the comparison of the core-level for hollow adsorbed

Table 8
Oxygen 1s core level energies for oxygen adsorbed for various coverage, sites (h—hollow, b—bridge, t—top, tet—tetrahedral sub-surface site, oct—octahedral subsurface site) and structures

Θ_O	Cell	Site(s)	$\Delta E_{CL}(O\,1s)$ [eV]
0.5	$c(2 \times 4)O_2$	h	+1.40
0.25	$p(\sqrt{2} \times 2\sqrt{2})$	h	≡0.00
0.25	$p(\sqrt{2} \times 2\sqrt{2})$	b	−1.36
0.25	$p(\sqrt{2} \times 2\sqrt{2})$	t	−1.88
0.25	$p(\sqrt{2} \times 2\sqrt{2})$	tet	−0.20
0.25	$p(\sqrt{2} \times 2\sqrt{2})$	oct	+0.45
0.50	$p(\sqrt{2} \times 2\sqrt{2})$	2×h	+0.01
1.00	$p(\sqrt{2} \times 2\sqrt{2})$	4×h	+0.61
0.50	mr-$p(\sqrt{2} \times 2\sqrt{2})$	2×h	+0.39
0.75	mr-$p(\sqrt{2} \times 2\sqrt{2})$	2×h + oct	+0.35/+0.21
–	Bulk-$p(\sqrt{2} \times 2\sqrt{2})$	tet	+0.22
–	Bulk-$p(\sqrt{2} \times 2\sqrt{2})$	oct	+0.91
–	Bulk Ag$_2$O-$p(\sqrt{2} \times 2\sqrt{2})$	–	+1.07
–	Ag$_2$O-$p(\sqrt{2} \times \sqrt{2})$–O-term	b/tet	−1.45/+0.57
–	Ag$_2$O-$p(\sqrt{2} \times \sqrt{2})$–Ag-term	tet	+0.35

All energies are given with respect to the binding energy of the hollow adsorbed species at low coverage.

oxygen at $\Theta = 0.25$ and 0.50 ML. Only for $\Theta = 1.00$ ML the binding energy is larger, since the special adsorption geometry slightly below the surface layer for this coverage leads to a higher "effective coordination number". Also the values for the missing row reconstructed surface have slightly higher binding energies compared to hollow adsorption. Again the low adsorption height increases the effective coordination and hence also the O 1s binding energy. The subsurface sites continue this trend: the oxygen binding energy of the lower coordinated tetrahedral site is 0.2 eV below that of the hollow adsorbed species, for the higher coordinated octahedral site the binding energy increases even more. The highest binding energy is calculated for the molecular state: in addition to the high-coordinated adsorption site there is a substantial oxygen–oxygen bond. The lower coordinated bridge and on-top adsorbed atoms continue the trend at the other end of the spectrum.

3.9. Optimal adsorption sites with increasing coverage: mixed surface and subsurface adsorption

To complete our study we investigated several more adsorption structures (in total more than 50 different structures) with mixed on-surface and sub-surface oxygen for total oxygen coverage between $\Theta = 0.11$ and 2 ML. The adsorption energy for a selection of adsorption structures as a function of oxygen coverage is plotted in Fig. 7. Up to half monolayer coverage the hollow site is the most favorable adsorption position; at $\Theta = 0.5$ ML only the missing-row reconstruction is degenerate with the c(2 × 2) structure (comp. Section 3.5). At higher coverage combinations of subsurface and on-surface sites become more stable: at $\Theta = 0.75$ ML a combination of two hollow and one octahedral sites in a p(2 × 2) cell, at full coverage half of the oxygen is located below the surface in octahedral sites and half of it on the surface in the hollow sites. Interestingly for adsorption in isolated sub-surface sites, the tetrahedral site is more stable (see Fig. 2). This is also true in combination with 1 ML of on-surface oxygen (see Fig. 7), but the octahedral site becomes clearly more favorable for higher sub-surface coverage.
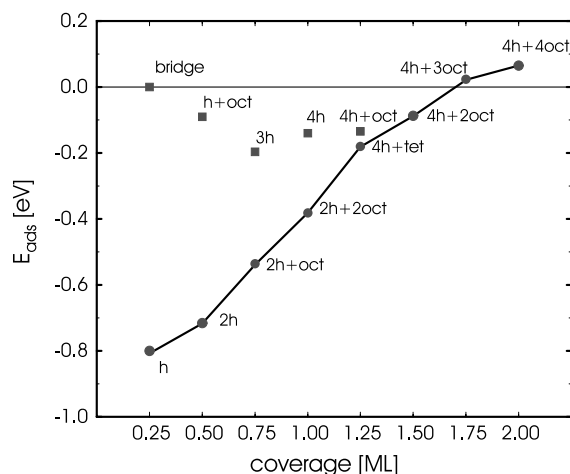

Fig. 7. Adsorption energy E_{ads} for the structures at the coverage from 0.25 to 2.0 ML calculated in a p(2 × 2) cell. The second favorite structure is indicated by squares.

4. Summary and discussion

4.1. Surface energy

In order to facilitate a direct comparison of all structures with a different number of Ag atoms in the surface (missing row reconstruction, silver oxide $Ag_2O, \ldots$), we use the (surface) grand potential, i.e. the Legendre transform of the generalized surface energy (Eq. (2)) with respect to the number of oxygen atoms

$$\omega(\mu_O) = \sigma - \frac{N_O}{A} \mu_O \tag{3}$$

where μ_O stands for the chemical potential of oxygen (with $\mu_O(O_2) \equiv 0$ eV). Via this transformation the dependence on the number of (oxygen) particles is transformed into a dependence on the chemical potential. So every structure is represented by a line, where the intercept at the ordinate equals the surface energy and the slope increases with coverage. In Fig. 8 this quantity is plotted. It describes the stability of different Ag–O structures as a function of varying oxygen chemical potential. For fixed temperature (partial pressure) the chemical potential scale is equivalent to partial pressure (temperature). A more detail description can be found in the paper by Reuter and Scheffler
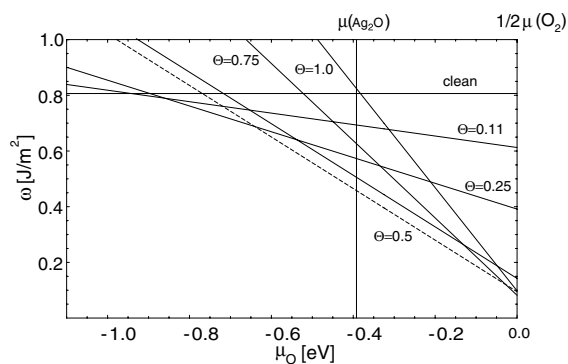
Fig. 8. Adsorption energy per area with respect to the chemical potential. Only the most favorite structures for each coverage (comp. Fig. 7) are shown). Additionally included is the half coverage missing row structure with a dashed line. $(1/2)\mu(O_2) = 0$ eV corresponds to free molecular oxygen and $\mu(Ag_2O) = -0.39$ eV to silver-oxide.

[43]. In the limit of low oxygen exposure (partial pressure, chemical potential) on the left hand side of the plot the clean silver surface exhibits the lowest grand potential and is hence the thermodynamically most stable structure. When the chemical potential increases to around −0.95 eV the thermodynamical equilibrium moves to the lowest investigated oxygen coverage ($\Theta = 1/9$ ML). With increasing chemical potential the p(2×2) structure at a quarter coverage becomes stable, followed by the two very similar half coverage structures (c(2×2) and missing row reconstruction). The calculated chemical potential of oxygen in the Ag_2O silver oxide structure (i.e. the heat of formation of the oxide) of −0.39 eV (experimental value: −0.32 eV [22]) represents the oxygen-rich limit for the investigated structures. In other words: for oxygen chemical potentials above −0.39 eV it is (from a thermodynamical point of view) more favorable to convert the silver surface into Ag_2O, than increasing the coverage at the surface beyond 0.5 ML.

The result of a maximum oxygen coverage of around 0.5 ML is consistent with the experimental estimate of a maximal coverage of around 0.4 ML [3]. Higher oxygen exposure leads already to an oxidation of the silver surface. This is also in line with the calculated core level binding energies.

4.2. Core-level energies

In Section 3.8.1 we demonstrated that there is a linear dependence between the Ag core level binding energy and the number of oxygen neighbors. The comparison with the experimentally determined core-level shift of ∼0.4 eV [3] implies that most silver surface atoms have only one oxygen neighbor. Only if also reconstructions, which reduce the coordination of the surface silver atoms are taken into account also two oxygen neighbors become possible (comp. Fig. 5). The results for the oxygen 1s binding energies are less simple to interpret.

Fig. 6 summarizes once more the experimental results. The main (low temperature) species is the hollow adsorbed oxygen species with a coverage less than 0.5 ML, which marks also the reference energy of the results compiled in Table 8. The molecular species is characterized by a higher binding energy; $\Delta E_{CL} \cong 1.4$ eV in our calculation compared to 1.7 eV in Ref. [3]. This discrepancy might be attributed to coverage effects for both the molecular and the atomic adsorbates. With increasing temperature Ag vacancies form and parts on the surface will undergo an oxygen-induced missing row reconstruction; perhaps with additional oxygen in residing in subsurface sites. Increasing the temperature even more the mobility within the surface layer also increases and the (experimentally observed) phase transition sets in, leading to two new peaks in the XPS signals at around 528.3 and 530.9 eV, i.e. at −2.0 and +0.6 eV with respect to the low temperature peak. The peak at −2.0 eV could indicate low-coordinated oxygen species (bridge, on-top sites). However, the energy difference between hollow and top sites is so large, that an occupation of on-top sites is highly unlikely at ambient temperatures. Bridge sites represent the saddle points for a diffusion between hollows—the calculated core-level shifts, however, are too small to account for the observed low-energy peak around 528.3 eV. It is more realistic to assume that the phase transition finally leads to the formation of an (oxygen terminated) oxide layer on top of the silver surface, characterized by oxygen atoms in bridge and tetrahedral interstitial sites of the silver substrate. The

calculated values of -1.45 and $+0.57$ eV for the perfect silver oxide layer agree reasonably well with experimental values (-2.0 and $+0.6$ eV), considering that the newly formed oxide is never perfectly flat and will not only consist of (100) facets, but also other surface orientations. Furthermore, the lattice constant will be determined by a compromise between that of the underlying silver substrate $a_{exp} = 4.08$ Å ($a_{GGA} = 4.16$ Å) and that of Ag$_2$O $a_{exp} = 4.72$ Å ($a_{GGA} = 4.83$ Å).

4.3. Work-function and frequencies

The results for work function and stretch frequencies provide further information. However, we are unable to explain the negative work-function change observed at low coverage and temperatures in Ref. [1]. The pronounced increase of the work-function with temperature and coverage is consistent with the higher values for $\Delta\Phi$ for the lower coordinated sites.

The adsorbate–substrate stretch frequencies for this particular system also do not permit a unique identification of the adsorption geometry. Both, the experimental and the calculated values, are biased by high uncertainties. On the experimental side the unknown coverage and different preparation methods lead to values differing by about 10%. For the calculation the strong coupling between soft surface modes of the substrate with the low vibrational frequencies of a relatively heavy adsorbate complicate the analysis. This mode coupling could only be taken into account by performing full ab initio molecular dynamics simulations over long time intervals.

4.4. Surface mobility

The high mobility of the silver surface is an important ingredient for its complicated behavior. Hence we want to spend a few words on this topic. During our study we performed additionally several ab initio molecular dynamics simulations, mainly for simulated annealing optimizations for various structures and surface stoichiometries. For example, by a simulation within a p($2\sqrt{2} \times 2$) cell with a surface stoichiometry of Ag:O $= 6:3$, we were able to reproduce the missing row recon-

struction. An interesting byproduct of these simulations is the very high mobility of the surface silver atoms, induced by the strong weakening of Ag–Ag bonds due to the formation of strong Ag–O bonds. Although we cannot give a quantitative description of this behavior, in all our simulations the mobility of the silver atoms was much higher compared to that of the oxygen atoms, which were hardly leaving their hollow sites. This observation is further supported by STM observations of a high mobility of Ag(100) surfaces under atmospheric conditions at room temperature [44]. This mobility favors the formation of vacancies and other defects well below the melting temperature, so that the effective silver coordination of the oxygen atoms is reduced. The consequence is an early onset of the metal–oxide transition accompanied by a variety of defects and small facettes exhibiting different orientations of the metal as well as the oxide surface. All this complicates the comparison with well defined surface structures as investigated in a theoretical study.

5. Conclusion

We have presented detailed ab initio density-functional studies of the atomic structure, energetics, and other properties of the clean and oxygen covered Ag(001) surface. Besides adsorption in high symmetry positions also molecular adsorption, an oxygen-induced missing-row reconstruction and the Ag$_2$O silver oxide surface was investigated. In comparison with data taken from the experimental literature we find the following scenario: at low temperature oxygen adsorbs molecularly, forming a c(2×4) over layer of molecules residing in hollow sites. At about 200 K these molecules dissociate. The atoms adsorb at hollow sites with coverages never exceeding 0.5 ML. Due to the strong Ag–O bond, the intermetallic bonds are weakened and partially broken, so that vacancy structures such as the missing row structure become possible. At even higher temperatures (around 320 K), all atoms at the surface become mobile, so that during silver diffusion the coordination number of the oxygen adsorption sites is reduced to three or even two. With increasing

oxygen exposure and temperature the silver surface turns into an Ag_2O surface covered with bridging oxygen atoms. By comparison with experimental findings [3], we propose that this species is finally the reactive one for e.g. CO or C_2H_4 oxidation.

Acknowledgements

References

[1] H.A. Engelhardt, D. Menzel, Surf. Sci. 57 (1976) 591.
[2] C.S. Ares Fang, Surf. Sci. Lett. 235 (1990) L291.
[3] M. Rocca, L. Savio, L. Vattuone, U. Burghaus, V. Palomba, N. Novelli, F. Buatier de Mongeot, U. Valbusa, Phys. Rev. B 61 (1) (2000) 213.
[4] F. Buatier de Mongeot, A. Cupolillo, M. Rocca, U. Valbusa, Chem. Phys. Lett. 302 (1999) 302.
[5] G. Benedek, F. Buatier de Mongeot, U. Valbusa, M. Rocca, Europhys. Lett. 53 (2001) 544.
[6] St. Messerli, S. Schintke, K. Morgenstern, J. Nieminen, W.-D. Schneider, Chem. Phys. Lett. 328 (2000) 330.
[7] F. Buatier de Mongeot, A. Cupolillo, U. Valbusa, M. Rocca, J. Chem. Phys. 106 (1997) 9297.
[8] F. Buatier de Mongeot, M. Rocca, A. Cupolillo, U. Valbusa, H.J. Kreuzer, S.H. Payne, J. Chem. Phys. 106 (1997) 711.
[9] L. Savio, L. Vattuone, M. Rocca, V. De Renzi, S. Gardonio, C. Mariani, U. del Pennino, G. Cipriani, A. Dal Corso, S. Baroni, Surf. Sci. 486 (2001) 65.
[10] S. Schintke, S. Messerli, K. Morgenstern, J. Nieminen, W. Schneider, J. Chem. Phys. 114 (9) (2001) 4206.
[11] G. Cipriani, D. Loffreda, A. Dal Corso, S. de Gironcoli, S. Baroni, Surf. Sci. 501 (2002) 182.
[12] Y. Wang, L. Jia, W. Wang, K. Fan, J. Phys. Chem. B 106 (2002) 3662.
[13] W.-X. Li, C. Stampfl, M. Scheffler, Phys. Rev. B 65 (2002) 075407.
[14] W.-X. Li, C. Stampfl, M. Scheffler, Phys. Rev. B 67 (2003) 045408.
[15] http://cms.mpi.univie.ac.at/vasp/.
[16] G. Kresse, J. Furthmüller, Phys. Rev. B 54 (1996) 11169.
[17] P. Blöchl, Phys. Rev. B 50 (1994) 17953.
[18] G. Kresse, D. Joubert, Phys. Rev. B 59 (1999) 1758.
[19] J.P. Perdew, A. Zunger, Phys. Rev. B 23 (1981) 5048.
[20] J.P. Perdew, J.A. Chevary, S.H. Vosko, K.A. Jackson, M.R. Pederson, D.J. Singh, C. Fiolhais, Phys. Rev. B 46 (1992) 6671.
[21] K.P. Huber, G. Herzberg, Molecular Structure and Molecular Spectra IV: Constants of Diatomic Molecules, Van Rostrand-Reinhold, New York, 1979.
[22] R.C. Weast, Handbook of Chemistry and Physics, 55th ed., CRC press Inc., 1982.
[23] G. Mills, H. Jónsson, G.K. Schenter, Surf. Sci. 324 (1995) 305.
[24] A. Ulitsky, R. Elber, J. Chem. Phys. 92 (1990) 1510.
[25] L. Köhler, Diploma Thesis, University of Vienna, 2002.
[26] J.R. Smith, F.J. Arlinghaus, J.G. Gay, Phys. Rev. B 22 (10) (1980) 4757.
[27] K.P. Bohnen, K.M. Ho, Surf. Sci. Rep. 19 (1993) 99.
[28] M. Methfessel, D. Hennig, M. Scheffler, Phys. Rev. B 46 (8) (1992) 4816.
[29] H. Li, J. Quinn, Y.S. Li, D. Tian, F. Jona, Phys. Rev. B 43 (9) (1991) 7305.
[30] H. Erschbaumer, A.J. Freeman, C.L. Fu, R. Podloucky, Surf. Sci. 243 (1991) 317.
[31] K. Giesen, F. Hage, F.J. Himpsel, et al., Phys. Rev. B 35 (3) (1987) 975.
[32] L. Vitos, A.V. Ruban, H.L. Skriver, J. Kollár, Surf. Sci. 411 (1998) 186.
[33] P.J. Van den Hoek, E.J. Baerends, R.A. van Santen, J. Phys. Chem. 93 (1989) 6469.
[34] M.C. Asensio, M.J. Ashwin, A.L.D. Kilcoyne, D.P. Woodruff, A.W. Robinson, Th. Lindner, J.S. Somers, D.E. Ricken, A.M. Bradshaw, Surf. Sci. 236 (1990) 1.
[35] M. Kittel, M. Polcik, R. Terborg, J.-T. Hoeft, P. Baumgärtel, A.M. Bradshaw, R.L. Toomes, J.-H. Kang, D.P. Woodruff, M. Pascal, C.L.A. Lamont, E. Rotenberg, Surf. Sci. 470 (2001) 311.
[36] L. Vattuone, P. Gambardella, U. Valbusa, M. Rocca, Surf. Sci. 377–379 (1997) 671.
[37] B. Hammer, L.B. Hansen, J.K. Nørskov, Phys. Rev. B 59 (1999) 7413.
[38] H. Over, Y.D. Kim, A.P. Seitsonen, S. Wendt, E. Lundgren, M. Schmid, P. Varga, A. Morgante, G. Ertl, Science 287 (2000) 1474.
[39] B.L.M. Hendriksen, J.W.M. Frenken, Phys. Rev. Lett. 89 (2002) 46101.
[40] R.W.G. Wyckoff, Cryst. Struct. 1 (1964) 331.
[41] A. Deb, A.K. Chatterjee, J. Phys.: Condens. Matt. 10 (1998) 11719.
[42] S. Lizzit, A. Baraldi, A. Groso, K. Reuter, M.V. Gandu-glia-Pirovano, C. Stampfl, M. Scheffler, M. Stichler, C. Keller, W. Wurth, D. Menzel, Phys. Rev. B 63 (2001) 205419.
[43] K. Reuter, M. Scheffler, Phys. Rev. B 65 (2002) 35406.
[44] B. Wichmann, J.P. van der Eerden, H. Meekes, J. Gerritsen, Electrochim. Acta 37 (1992) 2331.